Study of heavy impurity poloidal asymmetries induced by ICRH in ASDEX Upgrade using SXR tomography reconstruction

D. Mazon[1], D. Vezinet[1], M. Sertoli[2], R. Bilato[2], F.J. Casson[2], C. Angioni[2], V. Bobkov[2], R. Dux[2], A. Gude[2], R. Guirlet[1], V. Igochine[2], P. Malard[1]

and the ASDEX Upgrade Team

[1] *CEA, IRFM F-13108 Saint Paul-lez-Durance, France*
[2]*Max-Planck-Institute for Plasma Physics, EURATOM Association, Garching, Germany*

Understanding of the mechanisms leading to non-homogeneous impurity distribution could be useful knowledge for the control of heavy impurity transport and the avoidance of its accumulation in the plasma center necessary for sustaining long-pulse H-mode. Poloidal asymmetries of heavy impurities such as those generated indirectly by minority Ion Cyclotron Resonance Heating (ICRH) have recently been observed in H-mode plasma in metallic tokamaks [1]. These asymmetries are usually not taken into account in experimental impurity transport studies, which usually assume impurity densities are constant on a given flux-surface.

This paper presents recent dedicated experiments performed in H-mode discharges at ASDEX Upgrade (AUG) to analyze the effect of ICRH on the tungsten 2D density profiles. Injection of tungsten was triggered by laser blow off ablation (LBO) in different scenarios with fixed plasma current. Scans in ICRH power (H-minority heating scheme) and deposition location (change in frequency and toroidal field) have been performed in order to study their effects on Low Field Side (LFS) - High Field Side (HFS) asymmetries. In the following we will concentrate on the analysis of one particular discharge (pulse #29022, Ip ~ 0.6 MA - $\bar{n}_e$ ~ 4.5 10^{19} m^{-2}, B_T = 2.3T, ICRH frequency 30 MHz) which presents the advantage to have clear evidence of laser blow off induced signals on Soft X-ray data. In this pulse a parallel study was conducted in order to compare the asymmetries produced by tangential Neutral beam Injection (NBI) on the tungsten density profiles. The opposite asymmetry effects induced by NBI and ICRH are visible from the data time traces of the AUG Soft X-ray diode diagnostic [2]. Fig 1 illustrates this observation, where the time evolution of 4 SXR lines of sight (LOS) from the bottom vertical camera (left figure), chosen symmetric from the reconstructed magnetic axis are compared (right). During the ICRH phase, the asymmetry position depends mainly on the ICRH resonance location. The most distant lines of sight (LOS) from the magnetic axis (red and blue lines) intercepting the same length of plasma present differences during ICRH phase while are similar during phases where only NBI is applied, giving by such potential evidence of an HFS asymmetry. A switch in ICRH power from 3 to 5MW at t=4.7s indicates that the ICRH

power does not seem to play any role in the asymmetry location. In order to keep the same temperature profile for a correct emissivity comparison, central Electron Cyclotron Resonance Heating (ECRH), was reduced from 1.4 to 0.7MW. For the LOS closer to the magnetic axis (green and orange LOS) the NBI power makes difference and visibly triggers asymmetry on the low field side when the power exceeds 5MW from 6s to 7s. In order to study the spatial distribution of the LFS-HFS asymmetry, Soft-X-ray emissivity profiles were recovered from an original minimum Fisher inversion technique used to perform a full 2D tomographic reconstruction [3]. The impurity density can be then evaluated from the change in the local emission after the laser blow-off (see [4] and [5]). In Fig 2 (left), tomographic reconstruction of the LBO injection during the NBI phase (t=2.72s) is presented. The obtained 2D distribution (background subtracted in order to visualize the LBO effects only) shows again clearly a LFS/ HFS asymmetry as can be seen on the profiles shown in fig 3 (left). This picture is obtained dividing in quadrants from the magnetic axis the tomographic reconstruction and taking all points in the LFS and HFS regions for an estimate of the dispersion. The W is localized in the LFS region thanks to the centrifugal effect [6].

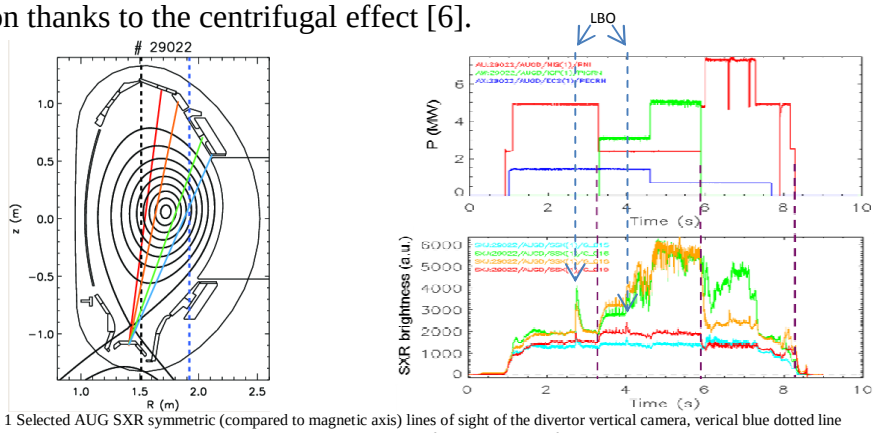

Fig 1 Selected AUG SXR symmetric (compared to magnetic axis) lines of sight of the divertor vertical camera, verical blue dotted line ICRH resonance location, black dotted line ECRH deposition location (left) time evolution of heating powers (blue line ECRH, red one NBI and green one ICRH) during #29022 discharge (top right) and related SXR data signals showing LFS/HFS asymmetries.

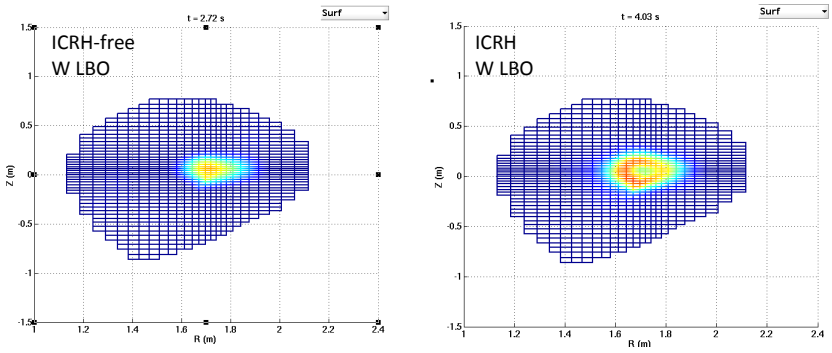

Fig 2 Tomographic reconstruction (background subtracted, background taken at 2,715s) for ICRH-free W LBO for pulse #29022 at 2.72s (left) and during ICRH W LBO (background taken at 4s) (right) for pulse #29022 at 4.03s.

For comparison the same kind of pictures are presented in Fig 2 (right) and Fig 3 (middle) for the LBO performed during the ICRH phase (t=4.03s). In this case the distribution is totally different. A HFS asymmetry is present up to 0.2 in normalized radius. Then, in the following

part of the profile we observe a light LFS asymmetry up to a normalized radius of 0.6 much less pronounced than in the NBI case. Assuming that the balance of ionization stages has little effect on the SXR emissivity, the W density can be deduced from the emissivity profile [5] (right plot in fig 3). The W density evaluation uses time-points at a similar relative distance from the sawtooth crash (present during this pulse) for more accurate background estimation. This profile is compared to simulation in the following.

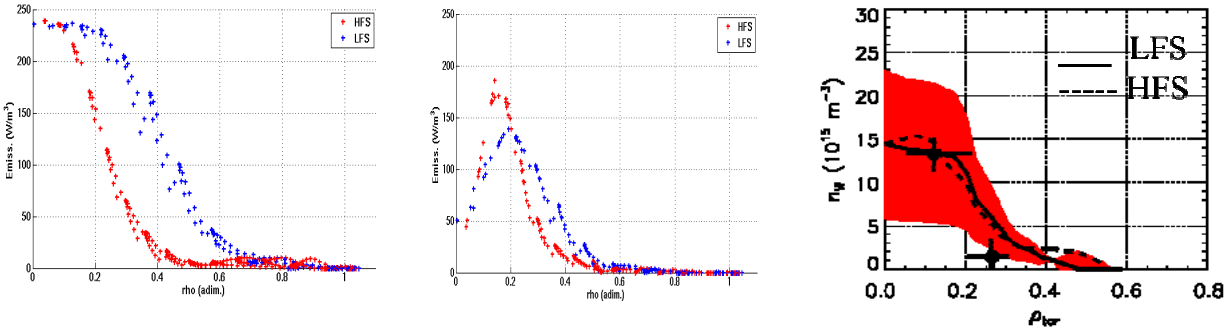

Fig 3 LFS/HFS asymmetry due to NBI for pulse #29022 at 2.72s (left), LFS/HFS asymmetry due to ICRH for pulse #29022 at 4.03s (middle). Simplified approach for fast estimation at t=4,03s of total W impurity density profiles from tomographic inversion assuming that the balance of ionization stages has little effect on the SXR emissivity [5], black dots with error bars are the measured W concentration from the grazing incidence spectrometer, error bars in red (right).

One of the leading mechanisms for explaining these ICRH poloidal asymmetries [1], [7] is analyzed using TORIC-SSPQL package [8] to estimate the temperature anisotropy of ICRH-heated minority species that could be at the origin of the observed asymmetries.

The W asymmetry is calculated from equation (8) of Reinke et al. paper [1], re-interpreted as

$$\frac{n_W}{< n_W >} = 1 + \frac{m_W \left(< R > \Omega \right)^2}{2T_i} \left(1 - Z_w \frac{m_D}{m_W} \frac{Z_{\text{eff}}\, T_e}{T_i + Z_{\text{eff}} T_e} \right) \left[\left(\frac{R}{< R >} \right)^2 - 1 \right]$$
$$- Z_W f_H \frac{T_e}{T_i + Z_{\text{eff}} T_e} \left[\left(\frac{R}{< R >} \right)^{\eta_H} - 1 \right]$$

Where deuterium mass, $m_D = 2m_p$ where m_p is the proton mass and the W mass: $m_W = 184m_p$. The core ionization for W is not a strong function of the temperature. On top of this, the range of ionization stages is always narrow. At 1.5keV plasma, the range is about Z=28-33 (Gaussian shape) and Z_w=31 is a good approximation of the total W at mid radius (see Fig 4 and Fig 5), and is within 25% at the core average value Z_w=40. The fraction of minority ions is set to f_H = 0.05. Finally the temperature anisotropy of the minority ion is given by $\eta_H = T_{H\ \text{perp}}/T_{H//} - 1$, from TORIC − SSFPQL code [8]. The plasma profiles used in the code are given in Fig 4. The plasma angular rotation frequency Ω is related to the toroidal velocity v_{tor} measured on the low field side: $\Omega = v_{tor}/R_{out}$. If the Mach number is defined as $M_D = vtor/(2T_i/m_D)^{1/2}$ and $< R > = R_0$ (magnetic axis major radius) is assumed, and from the previous equation the in-out density becomes:

$$\frac{n_W|_{\text{out}} - n_W|_{\text{in}}}{< n_W >} = \frac{m_W}{m_D} \left(\frac{R_0}{R_{\text{out}}} \right)^2 M_D^2 \left(1 - Z_w \frac{m_D}{m_W} \frac{Z_{\text{eff}}\, T_e}{T_i + Z_{\text{eff}} T_e} \right) \left[\left(\frac{R_{\text{out}}}{R_0} \right)^2 - \left(\frac{R_{\text{in}}}{R_0} \right)^2 \right]$$
$$- Z_W f_H \frac{T_e}{T_i + Z_{\text{eff}} T_e} \left[\left(\frac{R_{\text{out}}}{R_0} \right)^{\eta_H} - \left(\frac{R_{\text{in}}}{R_0} \right)^{\eta_H} \right]$$

Fig 5 shows the asymmetry predicted by this formula for the particular ion W^{31+} (pulse #29022 at 4s) for two values of Z_{eff}. As reference the dashed line shows the case without temperature anisotropy showing a clear LFS asymmetry due mainly to NBI. Despite the fact that only one ionization state of W is considered, good agreement with experimental W distribution, in particular in the region 0.15 to 0.6 is found (despite small change due to the definition of the radial coordinate inherent to the codes).

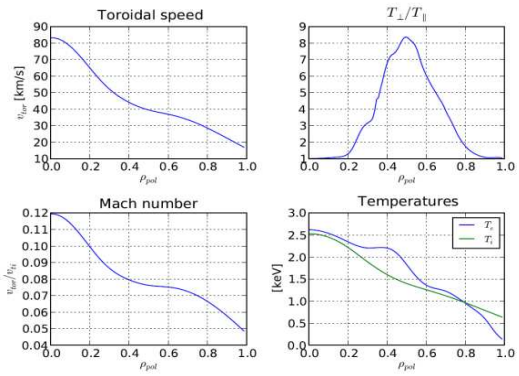

Fig 4 Main plasma profiles necessary to estimate the W density asymmetry according to [1] v_{tor}, T_i from CXRS signals and T_e from IDA [9].

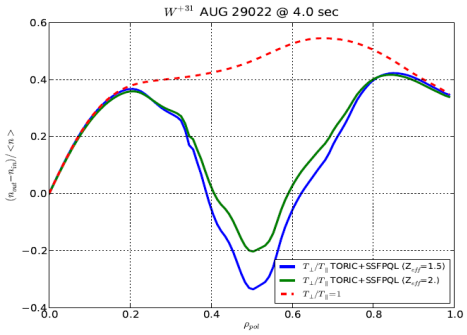

Fig 5 W density asymmetry (n_{Wout}-n_{Win}) according to [1] for two values of Z_{eff}. As reference, the dashed line shows the case without the temperature anisotropy.

Indeed from simulation we find a LFS asymmetry of about 30% maximum from 0 to 0.4 in normalized radius (we had ~15% of LFS asymmetry from the experimental results from 0.15 to 0.35). Then from 0.4 to 0.6 where ICRH is deposited (respectively 0.35 to 0.6 for experimental data) we observe a HFS asymmetry. Outside 0.6 a LFS asymmetry is seen from the model but no exploitable data from SXR data where signal is too low to confirm this.
In conclusion experimental evidences of both LFS and HFS asymmetry triggered respectively by NBI and ICRH power have been observed on AUG from SXR measurement. Laser blow off ablation authorized finer analyses and comparison between the two mechanisms using tomographic inversion. Simulation of the ICRH driven asymmetry confirmed the subsequent mechanism found in previous publication and the theoretical formula describing such asymmetry, at least in the surrounding of the deposition location. Nevertheless, these preliminary results need to be confirmed with further sensitivity checks. More precise comparison between simulation and experimental data are in preparation.

References:

[1] M. L. Reinke et al., Plasma Physics and Controlled Fusion **54** (4), 045004 (2012)
[2] V. Igochine et al., Internal IPP report: IPP 1/338 (2010)
[3] D. Mazon et al., Review of Scientific Instruments **83**(6), 063505 (2012)
[4] M. Sertoli et al., Plasma Physics and Controlled Fusion **53**(3), 035024 (2011)
[5] D. Vezinet et al., Fusion Science and Technology **63** (1), 9-19, (2013)
[6] J. Wesson et al., Nuclear fusion, **37**, 577, (1997)
[7] L C Ingesson et al., Plasma Physics and Controlled Fusion **42**, 161-180 (2000)
[8] R. Bilato et al., Nuclear Fusion **51**, 103034 (2011)
[9] R. Fischer et al., Fus Science and Techn **58**, 2, 675-684, (2010)